MEDICAL NOW Digest

No.86 2019

SHIMADZU

CONTENTS

This booklet is a digest version of MEDICAL NOW No. 86 (Published in August 2019), which is issued for Japanese medical professionals.

Feature Article

The Front Line in Osteoporosis Diagnosis

Teruki Sone, M.D., Ph.D.

Department of Nuclear Medicine, Kawasaki Medical School
Teruki Sone

1. Introduction

Osteoporosis diagnosis requires a noninvasive method of estimating bone strength, and bone strength evaluation is particularly essential to diagnose osteoporosis and start treatment before fractures occur. Bone mineral density measured by dual-energy X-ray absorptiometry (DXA) is currently used as an indicator of bone strength. However, the reduced bone strength in osteoporosis is defined not only by reduced bone mineral density but also by factors collectively called “bone quality” such as bone geometry, microarchitecture, microfractures, metabolic turnover, and degree of bone calcification (Fig. 1). Here we briefly describe current methods of evaluating bone strength used in clinical practice including measurement of bone mass.

Bone strength = Bone mineral density + Bone quality (structure and material quality)

Bone microarchitecture
Bone metabolic turnover
Microfracture
Bone calcification

Fig.1 The effect of bone mineral density and bone quality on bone strength
Although bone mineral density accounts for around 70% of bone strength, the effects of other factors cannot be ignored.

2. Clinical Methods of Bone Strength Evaluation and Characteristic Features

2.1 Bone Mineral Density Measurement

Bone density, which is said to determine as much as 70% of bone strength, is obtained by bone mass measurement. Some methods of measuring bone mass include DXA by X-rays, quantitative CT (QCT), radiographic absorptiometry (RA), and quantitative ultrasound (QUS) by ultrasonography. RA and QUS can both measure bone mass in peripheral bones (RA: metacarpus, QUS: calcaneus, forearm bone, etc.) while DXA and QCT can measure bone mass in peripheral bones as well as the lumbar spine and the proximal femur. All of these are established methods of measuring bone mass that are still seeing improvements in accuracy and convenience.

2.2 Evaluation of Macroscopic Bone Morphology

Methods of evaluating bone morphology have long been considered in terms of the relationship between morphological measurements and risk of proximal femoral fracture. Femoral neck-shaft angle and neck length (hip axis length, HAL) correspond to the methods. Recently, the method to quantify the cross-sectional shape of the proximal femur (hip structure analysis, HSA) has been developed and is utilized as a tool in clinical research and in clinical trials to evaluate bone strength in the proximal femur in terms of structure (Fig. 2). HSA provides indexes shown in Table 1 at the three sites of the femoral neck, the intertrochanter, and the femoral shaft, and these show slightly different patterns of aging-associated and osteoporosis treatment-associated change compared to bone mineral

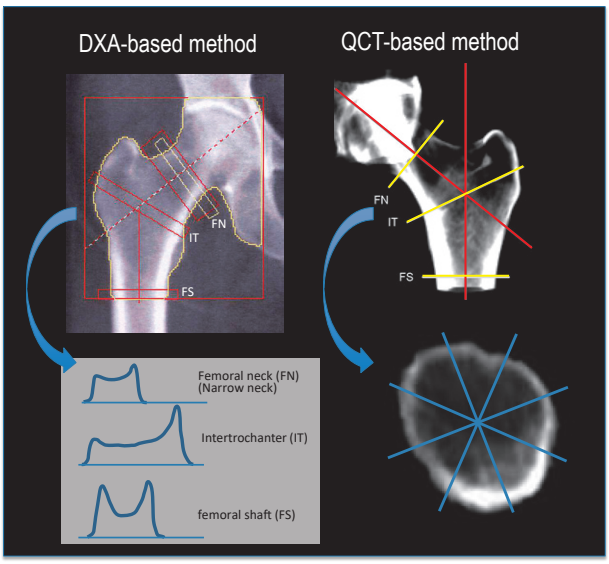

Fig.2 Strength analysis of the proximal femur (HSA) by CT and DXA.

density. Though the QCT-based method is more accurate, bone morphology can also be calculated based on the measurement data by DXA of the proximal femur.

Table 1. Indicators obtained by HSA

Bone outer diameter and cortical bone inner diameter
Mean cortical bone thickness
Bone cross-sectional area (area taken up by cortical and cancellous bone)
Second moment of area
Section modulus (indicator of strength against bending)
Buckling ratio (indicator related to strength against buckling)

2.3 Evaluation of Bone Microarchitecture

Bone structure imaging and analysis require image resolutions high enough for the intended application. For example, an image resolution of around 1 mm can be used to observe the shape of large bones, but an image resolution of around 100 μm is needed to observe the distribution of bone trabeculae.

Recent clinical CT can achieve image resolutions with a pixel diameter of 200 μm and a slice thickness of around 500 μm. Bone trabeculae width cannot be measured directly at this resolution, but bone microarchitecture can be evaluated quantitatively based on the distribution of cancellous trabeculae. For peripheral bones, high resolution peripheral quantitative CT (HR-pQCT), that is capable of an image resolution and slice thickness of 100 μm or less, is commercially available and used for quantitative evaluation of bone microarchitecture for cortical bone porosity and other characteristics.

Analytical software has been developed that calculates an indicator of cancellous bone structure (trabecular bone score, TBS) based on DXA scanning data. This software provides a simple method of evaluating cancellous bone structure and is currently being developed for clinical use (Fig. 3). TBS is a numerical indicator that is calculated based on the texture analysis of lumbar spine DXA images, and though this indicator has some limitations, it has attracted interests as a simple method of obtaining an indicator that correlates with cancellous bone microarchitecture.

2.4 Finite Element Analysis

Bone mass increases and decreases differently based on sites and localized factors such as stress risers at sites of reduced bone mass affect fracture occurrence. For this reason, fracture risk is determined based on a combination of bone strength and external force. Evaluations of fracture risk must therefore consider the size of the load on the bone as well as the site and direction of that load. Finite element analysis based on CT data (CT-FEM) creates a three-dimensional bone model from CT images of lumbar vertebrae or the proximal femur and predicts fracture risk based on sites where fractures start to occur when loading is increased under given conditions of mechanical loading and constraint, as well as based on the quantitative load when fracture starts to occur (Fig. 4). While CT image resolution is limited by the relationship between resolution and CT exposure dose, high-resolution data enables the acquisition and analysis of information on the microarchitecture of cancellous trabeculae.

2.5 Methods Other than Diagnostic Imaging

Apart from image-based diagnosis, other methods are being explored that are using blood and urine markers and measuring bone strength by microindentation.

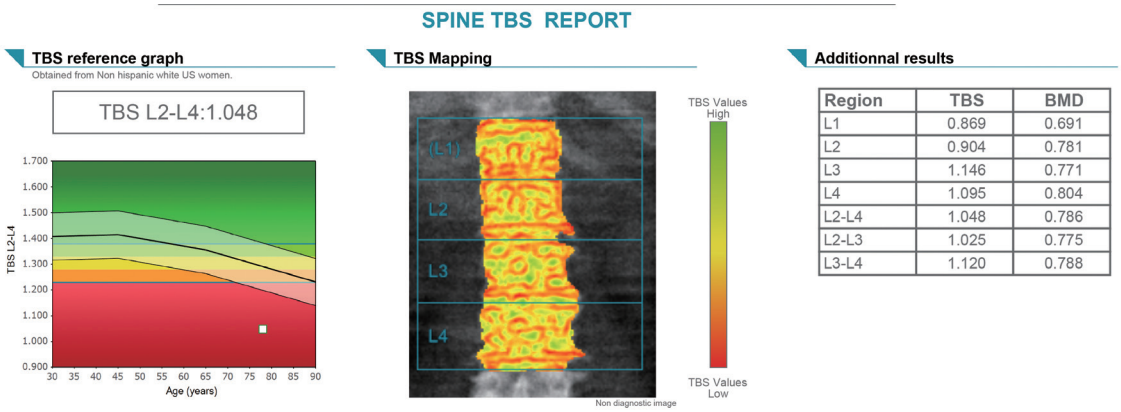

Fig.3 Evaluation of lumbar spine cancellous bone by DXA (TBS)
Results of analysis in a 78-year-old woman. Although L2–L4 BMD is still in the low bone mass range at 0.786 g/cm^2 (78 % of young adult mean, -1.9 T-score), TBS is markedly low at 1.048.

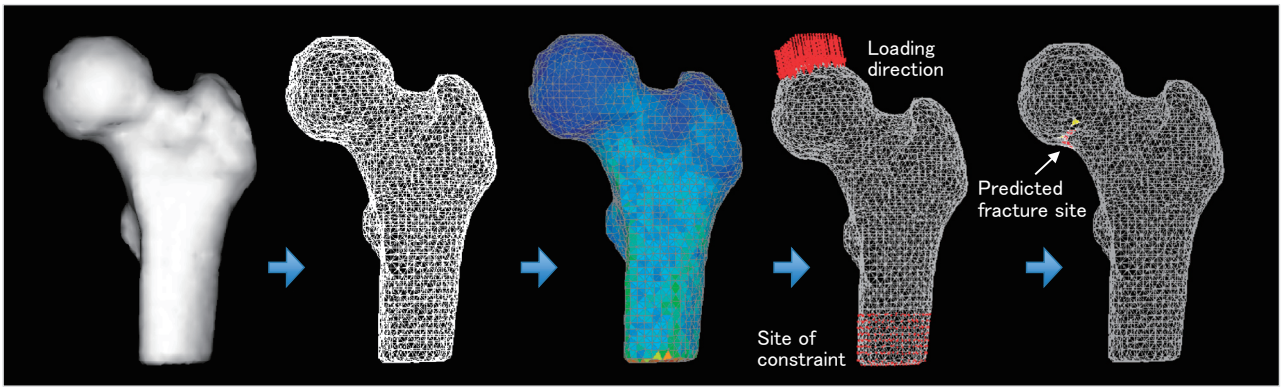

Fig.4 Predicting fracture loading by CT-FEM
Finite element analysis of CT data predicts fracture loading and fracture sites under given conditions of mechanical loading and constraint.

3. What Did New Methods Reveal?

3.1 Confirming the Utility of DXA-BMD as an Indicator of Bone Strength

One of the shortcomings of bone mass measurement by DXA is that bone mineral density is given in terms of unit surface area (areal bone mineral density, aBMD) and not unit volume. When two bones have identical volumetric bone mineral density (vBMD) but differ in size, the bigger bone will have a larger aBMD. This is considered to be the main reason that males have a larger aBMD than females. By contrast, epidemiological investigation has shown there is almost no sex-based difference in the relationship between DXA-based aBMD and fracture risk. Assuming a direct relationship between fracture risk and bone strength, the relationship between aBMD and bone strength should be almost identical in males and females.

According to a report using QCT of the proximal femur to investigate this relationship, aBMD is almost the same in males and females due to the fact that though males have larger bones than females, this size difference is balanced out by the smaller vBMD in males.[1] In addition, when calculated by CT-FEM, there is almost no sex-based difference in either bone strength or load-to-strength ratio (the ratio of strength to estimated load during a fall). CT-FEM-based investigations indicated that DXA-based bone density has become more significant as an index of bone strength as it contains the information of bone size.

3.2 Clinical Significance of Bone Geometry Indicators

Among the structural indices of the proximal femur, HAL is a different risk factor from bone mineral density of the proximal femur fracture. However, while HAL is used in epidemiological investigations of ethnic differences in fracture frequency, it is not used in osteoporosis to determine targets for therapeutic intervention.

HSA index was initially expected to be a clinical index that complements bone mineral density because of its association with fracture risk and its response to drug therapy. However, some HSA indicators, that are section modulus and buckling ratio in particular, are significant predictors of fracture but mainly used in clinical research because they are not so independent of bone mineral density and are also inferior to bone mineral density in terms of measurement reproducibility.

3.3 Age-Related Increase in Cortical Bone Porosity

Age is a risk factor for fracture that is independent of bone mineral density, but it has so far been difficult to observe differences in bone microarchitecture between young and elderly people who have equivalent bone mineral density in a clinical setting. According to findings from studies using HR-pQCT, among the indicators of cancellous bone microarchitecture such as trabecular width, trabecular number, cortical bone thickness and its porosity, cortical bone porosity particularly exhibits age-related changes that are independent of bone mineral density and suggests a relationship between lowering bone strength in the elderly.[2] In other words, though deterioration of bone

microarchitecture and decrease in bone mineral density progress with age, it's considered that the age-related changes of microarchitecture in cortical bone may be tending to be more independent of bone mineral density than the one in cancellous bone.

3.4 Utility and Limitations of Trabecular Bone Score (TBS)

Many study results have shown that TBS predicts fractures independent of bone mineral density in postmenopausal women. Also, incorporating TBS into FRAX® (WHO tool for evaluating fracture risk) increases the ability of FRAX® to predict fractures. For these reasons, TBS can be used to determine when to start drug treatment and expected to be helpful particularly for women near the therapeutic threshold according to existing standards and for women who are 65 years and younger.

A reduction in TBS is even seen in a variety of cases of secondary osteoporosis. Bone quality is generally considered to be a greater influence on reduction of bone strength in diabetes-induced and steroid-induced osteoporosis than in primary osteoporosis, and TBS is shown to be an effective indicator for evaluating bone strength in patients with these diseases.

The percentage change in TBS caused by osteoclastic inhibitors tends to be smaller than the one in bone mineral density, and the connection between fracture prevention and treatment-induced percentage change in TBS is also weaker than for bone mineral density. Consequently, TBS is not so suitable for evaluating the therapeutic effect of bisphosphonate and other osteoclastic inhibitors. As yet, no consensus has been reached on the change in TBS caused by agents that stimulate bone formation such as parathyroid hormone (PTH) or on the significance of such changes.

3.5 Clinical Significance of CT-FEM

CT-FEM is often considered the gold standard for clinical evaluation of bone strength and is used to analyze the detailed effects of drug treatment among other applications. For example, Keaveny et al. administered alendronate or teriparatide to patients with osteoporosis for 18 months then compared therapeutic effect by spine QCT.[3] Both alendronate and teriparatide increased vBMD and bone strength, but a larger percentage increase in vBMD and bone strength was observed with teriparatide than alendronate and there was a marked increase in cancellous bone with teriparatide. Furthermore, the percentage increase in bone strength/vBMD ratio was five times larger with teriparatide than alendronate and teriparatide was considered to be an effective means for increasing bone strength since it increases bone in the position which is important for the strength.

The general evaluation for the accuracy of CT-FEM is high, and International Society for Clinical Densitometry officially states that the ability of CT-FEM to predict vertebral body fractures is superior to bone mineral density determined by DXA, and the ability of CT-FEM to predict proximal femoral fractures is equivalent or better than bone mineral density determined by DXA.[4]

4. Conclusion

This article has described the current situation regarding methods of evaluating bone strength, which is an essential evaluating indicator in osteoporosis diagnosis. We look forward to these methods being utilized for pathological analysis of bone diseases, evaluation of fracture risk, and determining the therapeutic effect of drugs.

References

1) Srinivasan B, et al. Relationship of femoral neck areal bone mineral density to volumetric bone mineral density, bone size, and femoral strength in men and women. Osteoporos Int 2012; 23: 155-162.
2) Nicks KM, et al. Relationship of age to bone microstructure independent of areal bone mineral density. J Bone Miner Res 2012; 27(3): 637-644.
3) Keaveny TM, et al. Effects of teriparatide and alendronate on vertebral strength as assessed by finite element modeling of QCT scans in women with osteoporosis. J Bone Miner Res 2007; 22: 149-157.
4) Zysset P, et al: Clinical Use of Quantitative Computed Tomography-Based Finite Element Analysis of the Hip and Spine in the Management of Osteoporosis in Adults: the 2015 ISCD Official Positions-Part II. J Clin Densitom 2015; 18: 359-392.

Surgery

Our Experience Using LIGHTVISION for Lymphaticovenular Anastomosis

Akitatsu Hayashi, M.D.

Lymphedema Clinic, Department of Breast Center, Kameda Medical Center
Lymphedema Clinic, Kameda Kyobashi Clinic
Akitatsu Hayashi

1. Introduction

Kameda Medical Center boasts 380 years of history, 35 medical departments, and about 3,000 staff, and is a foundation hospital located in southern Chiba Prefecture that focuses mainly on providing acute phase advanced medical care **(Fig. 1)**. In 1995, Kameda Medical Center was the first facility in the world to implement a full-scale electronic medical record system and is known as one of the rare facilities in Japan that implements total information utilization for medical care. We are also fully committed to improving our quality of medical care, with all medical services, including the clinical section, ISO 9001 accredited and certified by the Japan Council for Quality Health Care. Furthermore, in 2009, we were the first facility in Japan to receive accreditation from the Joint Commission International (JCI) that evaluates health care systems and practices. Started in April 2013, the Kyobashi Clinic in Tokyo has also established a women's clinic and medical checkup facilities and provides medical care to foreigners and patients from Tokyo and throughout Japan.

In February 2018, our department of breast center started a lymphedema clinic to meet an increased demand for treatment of secondary lymphedema arising after surgery, radiotherapy, and chemotherapy for breast cancer. Until establishing the lymphedema clinic, our only option for treating lymphedema was to start conservative therapy once arms and legs had already become swollen. Now, a lymphedema specialist carries out examinations and imaging investigations for early discovery and treatment of lymphedema, and surgical treatment is also available for indicated patients. Typical surgical treatments for lymphedema include lymphaticovenular anastomosis and vascularized lymph node/vessel transplantation. Indocyanine green (ICG) plays a key role in all these surgeries for both preoperative and perioperative lymphography. ICG lymphography, or ICG fluorescence imaging, is a technique that allows observation of lymphatic vessels by irradiating ICG taken up by lymphatic vessels with near-infrared excitation light, which is visualized as near-infrared fluorescence emitted by ICG. The near-infrared camera system used by this technique can be arm-mounted or hand-held depending on the retention system, and in 2016, Shimadzu developed an arm-mounted LIGHTVISION near-infrared fluorescence imaging system that displays detailed high definition images. LIGHTVISION has been used at our facility since the spring of 2018 in over 100 cases and for over 300 lymphaticovenular anastomosis procedures. Here we report on our experience using Shimadzu's LIGHTVISION system.

Fig.1

2. What is Lymphaticovenular Anastomosis for Lymphedema?

Lymphatic vessels in the extremities normally follow an independent route until emptying into the left and right subclavian veins. However, in cases of secondary lymphedema following cancer surgery, there is gradual and progressive lymphatic vessel degeneration **(Fig. 2)** that causes lymphedema when lymph fluid flow is blocked at some point in

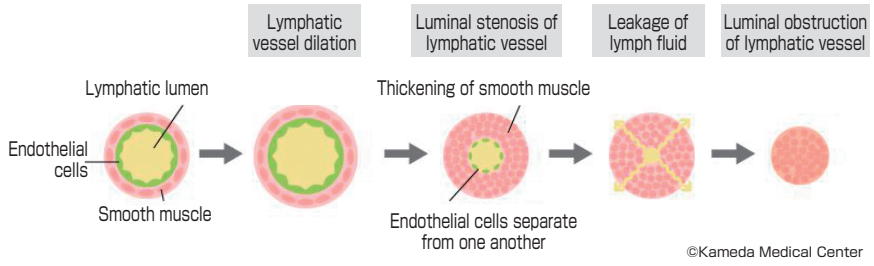

Fig.2

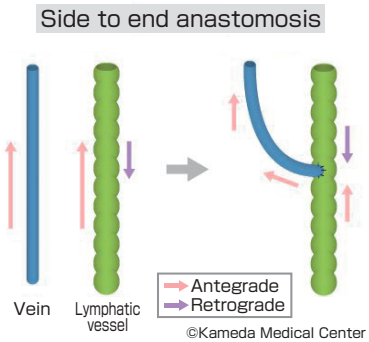

Fig.3

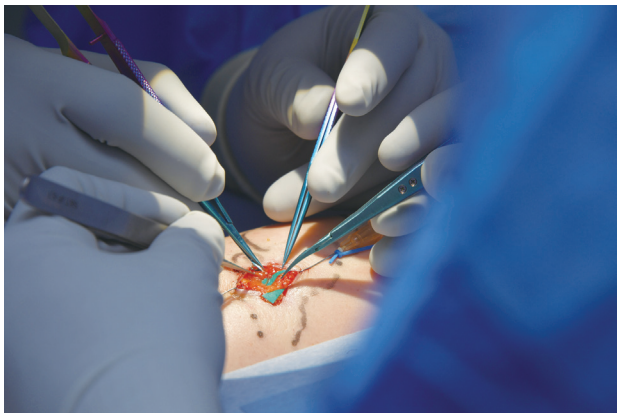

Fig.4

Fig.5

the vessel. Lymphaticovenular anastomosis is a functional reconstructive surgery that bypasses the lymph blockage and resolves lymph fluid stasis by redirecting lymph flow into the vein from a point in the lymphatic vessel distal to the blockage **(Fig. 3)**. The major technical challenge faced by this surgery was the extreme thinness of lymphatic vessels in the extremities (internal diameter of 0.2–1.0 mm), but recent improvements in surgical tools and techniques, such as forceps and threads designed for 50 μm ultra-fine vessel anastomosis **(Fig. 4)**, have resulted in the emergence of "supermicrosurgery" that can perform proper anastomosis of vessels under 0.5 mm diameter and has led to the development and evolution of lymphaticovenular anastomosis (LVA) in Japan, which is a procedure that performs anastomosis of the lymphatic vessel and venule endothelium. Progress has been made in reducing the risk of obstruction and thrombus formation at the anastomotic site and improving surgical outcomes for LVA, and interest in this surgery is currently spreading throughout the world due to the low invasiveness and the effectiveness of the procedure.

3. ICG Fluorescence Imaging in Lymphaticovenular Anastomosis

Preanastomosis lymphatic vessel selection is directly linked to success or failure of surgery and is, therefore, the most important step in LVA, and is where ICG fluorescence imaging comes into its own. ICG fluorescence imaging can visualize the flow dynamics of lymph fluid in lymphatic vessels and is one of the best methods we currently have for identifying lymphatic vessels for LVA. When lymphatic vessels appear as a linear pattern on ICG fluorescence imaging, it shows the visualized region of the vessel is still actively transporting lymph fluid. The ability to identify such lymphatic vessels with active flow during surgery is important, regardless of lymphedema severity. lymphatic vessels with active flow have undergone relatively little degeneration, are often easy to anastomotize, and tend to result in effective LVA. However, even after a linear pattern is verified following an initial injection of ICG, in patients with moderate or more severe lymphedema the region of lymph congestion can spread over time, creating dermal backflow patterns that obscure the linear patterns. In these situations, the identification of functional lymphatic vessel during surgery with ICG fluorescence

imaging becomes even more important.
In addition, stenosis at the site of anastomosis is also more common with supermicrosurgery than normal microsurgery, as supermicrosurgery performs anastomosis on vessels 0.5 mm and smaller in size. For these reasons, ICG fluorescence imaging is also important for evaluating surgery immediately after anastomosis to verify outflow into the anastomotized vein. Weak outflow or no outflow of ICG into the vein at this time indicates the anastomosis site is at high risk of obstruction and reanastomosis must be considered.
As such, ICG fluorescence imaging plays an extremely important role in lymphaticovenular anastomosis. At this hospital, after consent has been obtained from the patient, ICG fluorescence imaging is always used as part of lymphaticovenular anastomosis.

4. Characteristic Features of LIGHTVISION and Utility in Lymphaticovenular Anastomosis

First of all, LIGHTVISION is easy to use and easy to manipulate in surgery. The camera arm can be folded away during transit, extended during use, and allows free adjustment of the camera position. The camera arm extends up to around 180 cm and rotates horizontally through an angle of around 40 degrees, allowing the main unit to be positioned away from the operative field to ensure a wide range of movement around the patient and allow large microscopes used in surgeries like LVA to be positioned safely and with flexibility **(Fig. 6)**. The main unit is also equipped with a small display monitor and remote control so the operator can verify control and perform image quality adjustments, and allows the surgeon and operator to share images and continue with surgery without stress. Another major feature of LIGHTVISION is that imaging can be performed in an illuminated operating room allowing surgery to proceed in comfort and without stress.
One more major feature of this system is the simultaneous three-window display and display switching function. Visible light images, near-infrared images, and visible light + near-infrared images acquired by the image sensor can be shown simultaneously on the three-window display to allow verification and comparison of each image at a glance, even during surgery. For example, when three lymphatic vessels are within the field of view, the three-window display allows immediate determination of which lymphatic vessel is functional and the location of the functional lymphatic vessel without the need to switch between image views or compare with a microscope field of view **(Fig. 7)**. The image displayed in the largest window can also be changed easily, and our surgeons are pleased with the ability to quickly view the images they need to **(Fig. 8, 9)**.
Finally, I would like to mention the safety of the system. Although this system operates at a camera-to-subject distance of 500–700 mm, the system is equipped with a strong zoom function and displays very detailed, high definition images that can verify flow in even very fine lymphatic vessels of 0.2 mm or smaller diameter. Compared to microscope platforms capable of fluorescence imaging that are often used in lymphatic surgery, we found lymphatic vessels were identified clearly by LIGHTVISION in 12 cases that the microscope platform either failed to identify or identified only poorly. While it is convenient to have fluoroscopic imaging functions on a microscope, the short distance between the microscope and subject presents a constant risk of burning or damaging skin or tissue that is a constant concern for the surgeon. LIGHTVISION allows for safer and more accurate identification of lymphatic vessels and evaluation of anastomosis sites.

Fig.6


Fig.7

Fig.8

Fig.9

5. Conclusion

The use of lymphaticovenular anastomosis for lymphedema following cancer surgery has spread widely in the last few years. In this time, we have learned that lymphatic vessel selection before anastomosis has a major effect on postoperative outcomes. We think that LIGHTVISION, which allows for safe and highly accurate lymphatic vessel selection and evaluation after anastomosis, is extremely useful for either facilities that use microscopes equipped with fluorescence imaging functions, or in facilities that only have normal microscopes. Of the near-infrared fluorescence camera systems, LIGHTVISION is the only system that produces color images in high definition and we expect LIGHTVISION to become an indispensable tool in lymphedema surgery.

References

1) Koshima I, Inagawa K, Urushibara K, Moriguchi T. Supermicrosurgical lymphaticovenular anastomosis for the treatment of lymphedema in the upper extremities. J Reconstr Microsurg. 2000;16:437–442.
2) Yamamoto T, Yamamoto N, Yoshimatsu H, et al. Factors Associated with Lymphosclerosis: An Analysis on 962 Lymphatic Vessels. Plast Reconstr Surg. 2017;140:734-741.
3) Hayashi A, Hayashi N, Yoshimatsu H, et al. Effective and efficient lymphaticovenular anastomosis using preoperative ultrasound detection technique of lymphatic vessels in lower extremity lymphedema. J Surg Oncol. 2018 Feb; 117 (2):290-298

Advanced Healthcare

Development of Adrenal Venous Sampling (AVS) Support System for Primary Aldosteronism

Medical Systems Division, Shimadzu Corporation
Daisuke Notohara

1. Introduction

Primary aldosteronism (PA), the most common type of secondary hypertension, accounts for about 10% of the estimated 40 million cases of hypertension in Japan and is said to be two to twelve times more likely to result in complications than essential hypertension.[1)] Primary aldosteronism occurs when one or both adrenal glands secrete excessive amounts of a certain hormone called aldosterone. Unlike essential hypertension, which accounts for 90% of cases and can have a wide variety of causes, primary aldosteronism is considered hypertension that can be completely cured by treating the adrenal glands.

Basically, adrenal venous sampling (AVS) is performed to identify the area inside the adrenal gland that is secreting too much aldosterone. AVS involves using an angiography system to insert a catheter up to the left and right adrenal veins, so that blood can be selectively sampled from the adrenal veins. Then the blood acquired from the adrenal veins is analyzed to diagnose primary aldosteronism, but that process involves the following two issues.

- **Speed of Adrenal Vein Blood Analysis**
  Typically, blood is acquired from the adrenal veins and then the hormones aldosterone and cortisol are quantitated by the immunoassay method (immunological measurement method). Such measurements are typically performed at an external testing laboratory, which can take several days before results are obtained and makes it difficult to determine analysis results on the same day as AVS examinations.

- **Hand-Written Records of Blood Acquisition Locations and Analytical Results**
  To precisely determine the area of excessive aldosterone secretion, blood must be acquired selectively from several locations in the left and right adrenal veins. That requires recording a combination of the acquisition positions in the blood vessel, the ID numbers of the blood collection tubes where each blood sample was placed, and the results of hormone analysis. Normally, hand-written anatomical information and numeric data are managed separately.

Tohoku University has been involved in that type of super-selective adrenal venous sampling for many years. Given that Shimadzu Corporation has extremely advanced technology for not only medical systems, but also analytical and measuring instruments, Tohoku University worked with Shimadzu to jointly develop new solutions for performing blood analysis more quickly and integrating images with medical records.

2. Description of Technology

The AVS support system (for research use) developed for integrating X-ray images and localized blood analysis results is shown in **Fig. 1**. The system comprises a Shimadzu liquid chromatograph mass spectrometer (LCMS) system, AVSsolution software, which is newly developed LCMS data analysis software that was optimized for AVS, and Sampling Viewer software, which creates records that integrate analytical results with DICOM images acquired with an angiography system. Because the AVSsolution software can provide reference values for analysis results within the same day of AVS examination, measurements can be performed quickly. Furthermore, recording reference images with the blood acquisition position indicated in X-ray images (DICOM images) using the Sampling Viewer software and creating AVS reports can help improve workflow efficiency. The use of digital technology can be expected to prevent human errors as well.

Fig.1 AVS Support System Developed for Integrating X-Ray Images with Localized Blood Analysis Results (for Research Use)

Next, an example of workflow using the AVS support system is shown in Fig. 2. First, X-ray images (DICOM images) acquired by the angiography system are sended into Sampling Viewer. Then the blood collection tube ID information is loaded and recorded at the corresponding position in the X-ray image where the blood was acquired. That provides a record of which collection tube contains the blood acquired from any particular position in the vein. Next, the blood collection tube is carried to the LCMS system, where the same collection tube ID information is loaded and the data is analyzed to determine the quantity of aldosterone and cortisol in the blood, as shown in Fig. 3. LCMS enables selective detection and rapid sample measurement based on mass information about target compounds.

The LCMS system and Sampling Viewer software communicate via the hospital's internal network, so that analysis results are automatically recorded in Sampling Viewer. Eventually, Sampling Viewer

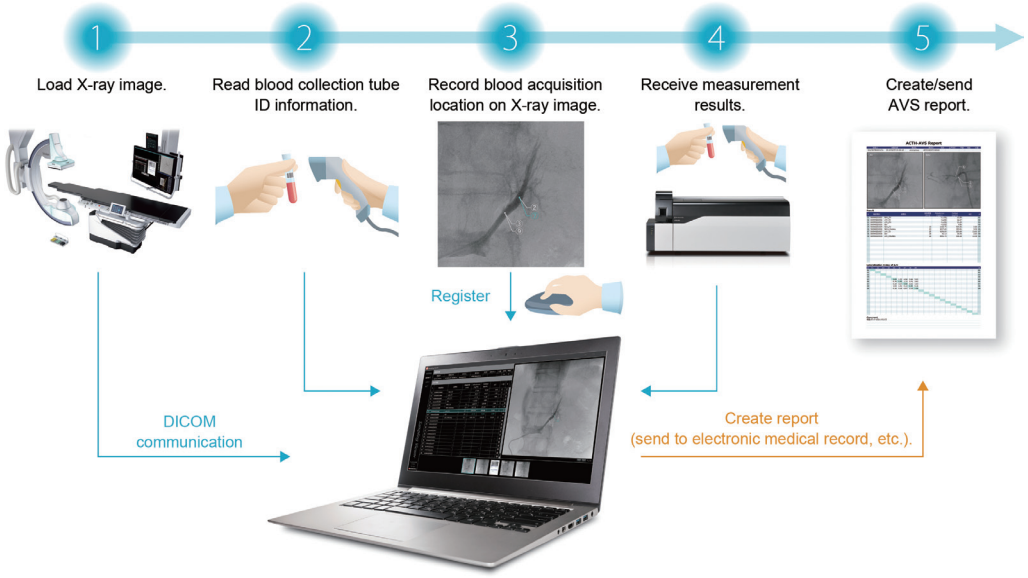

Fig.2 Example of AVS Support System Workflow

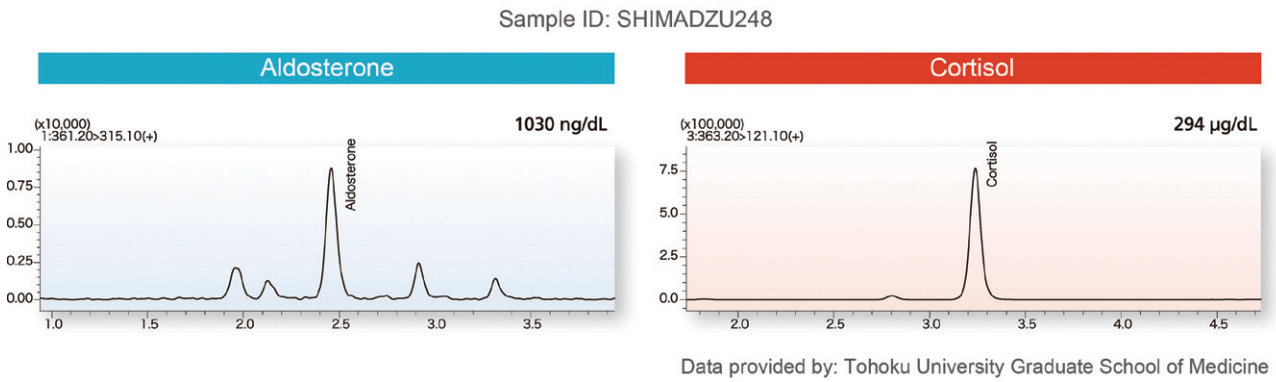

Fig.3 Example of LCMS Aldosterone and Cortisol Analysis

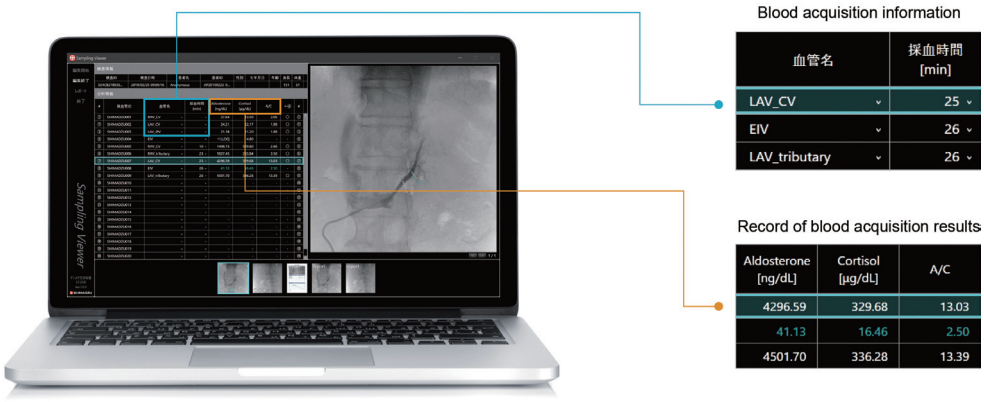

Fig.4 Example of Integrated Record from Sampling Viewer

creates an integrated record that includes the positions where blood was acquired, collection tube ID information, and analytical results, so that all the information can be confirmed in one location (Fig. 4).

3. Summary

The AVS support system described in this article was developed for the purpose of creating new solutions based on the integration of Shimadzu's core medical systems technologies with analytical and measuring instruments technologies. The project initially started when several Shimadzu engineers visited Dr. Kei Takase, a professor of Department of Diagnostic Radiology at the Tohoku University School of Medicine, in July 2015 to search for unmet needs in the healthcare field. That is when we learned about primary aldosteronism and carefully toured their workplace, which later led to the joint research project. To generate new concepts for healthcare equipment development, we need to continue fostering such close partnerships with healthcare facilities, rather than only with companies. Lastly, I would like to use this opportunity to sincerely thank Dr. Takase and others for allowing our engineers to keep visiting their workplace and for the many helpful suggestions they provided for this development project.

Reference:

1) Kei Takase, "IVR Technology for Curing Hypertension—Minimally Invasive Treatment for Primary Aldosteronism Using Adrenal Venous Sampling Technology—," Clinical Research, Innovation and Education Center, Tohoku University Hospital
https://www.crieto.hosp.tohoku.ac.jp/seedlist/seed01.html (referenced in May 10, 2019)

Note: The software and LCMS-8050 liquid chromatograph mass spectrometer described in this article have not been approved or certified as a medical product or medical device for in vitro diagnostic purposes under the Japanese Pharmaceutical and Medical Device Act. Therefore, they cannot be used for medical diagnostic purposes or associated procedures.

Minimally Invasive Procedures in Practice

—Effort by Fukuoka Kieikai Hospital Part 2—

Medical Systems Division, Shimadzu Corporation
Hiroyuki Kinoshita

Given the conplication and sophisticated interventional procedures in recent years, users are requesting angiography systems that can achieve lower X-ray dose levels, less required contrast agent, and shorter examination times. Shimadzu's latest Trinias series angiography system has various features for achieving minimal invasive procedures.

Continuing from the previous article, Part 2 of this series highlights uses of various functions for neurointerventional radiology and describes efforts made by Trinias at Fukuoka Kieikai Hospital.

1 Using Low-Dose Fluoroscopy Mode

Keeping the X-ray dose at the minimal level is important both for patients and physicians, particularly in the case of neurointervention. It is desirable to manage the exposure dose of not only the radiation exposure of a skin, but also the exposure of the crystalline lens, which has the deterministic effect.

At Fukuoka Kieikai Hospital, radiological technologists work together with physicians to achieve low dose practices. Although a fluoroscopy program of 10 pps[*1] is often used in neurointerventional procedure, they use 10 pps/Low (low-dose 10 pps mode). This mode reduces the X-ray dose by around 48 % and achieves a remarkable decrease insubstantial dose of X-ray **(Fig. 1)**. Use of the mode has been highly evaluated as follows, "The X-ray dose reduction is effective, and loss of image quality is permissible."

*1 pps: pulse per second

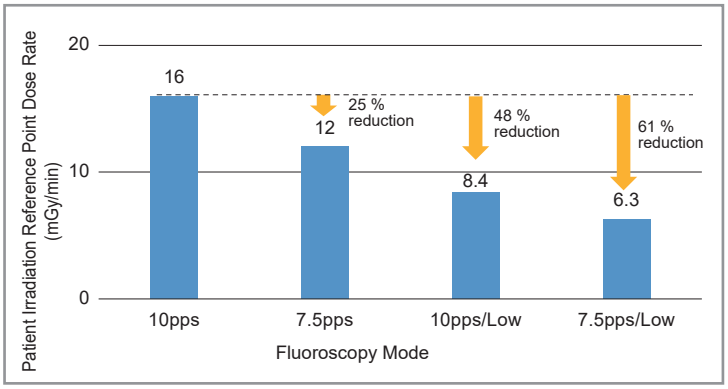

Fig. 1 Dose Rate Compared by Fluoroscopy Mode
Patient irradiation reference point dose rate for 12-inch field of view and 20 cm of acrylic
* Actual measurements taken with a Shimadzu system

2 Using Flex-APS that Automatically Corrects for Body Movement

Cerebral arteries have penetrating branches and other microscopic blood vessels that are just 0.1 to 0.5 mm in size. The presence and distribution of these vessels have a major effect on a treatment strategy. However, even slight movements of the patient' s body during DSA will cause misregistration artifacts that substantially reduce the visibility of blood vessels.

They use the original Flex-APS function of Trinias series unity edition to minimize the occurrence of the artifacts. Flex-APS is a function that, in real-time, corrects the artifacts in DSA images caused by patient body movements in real time[1] **(Fig. 2)**. Flex-APS differs from previous correction functions. It processes individual pixels, and allows to correct motion generated by three-dimensional twisting and motion caused by jaw movements in one area of an image. The

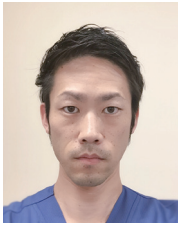

Comments of Ryosuke Abe, R.T., Department of Radiology

Our hospital introduced the Trinias B12 unity edition in June last year as construction completed on our new hospital site.

The Trinias has a variety of functions and we especially highly evaluate the Flex-APS. It is quite useful because it provides not only excellent DSA images but also high quality road map images as well.

In addition, we create merged image of vessels(artery & vein) and bones using 3D-DSA and CBCT data to create fusion images for better understanding of the positional relation of vessel structures with cases of tumor embolization procedure done before a tumor removal surgery. The workstation is also easy to operate and can create useful images in a short period of time.

function requires no special manipulation, and the image processing is applied automatically in real-time, so it does not interrupt the treatment procedures. Flex-APS has been appraised as follows, “Even when there is patient movement during the procedure, penetrating branches and other microscopic blood vessels that used to be difficult to observe can now be seen clearly on DSA images.”

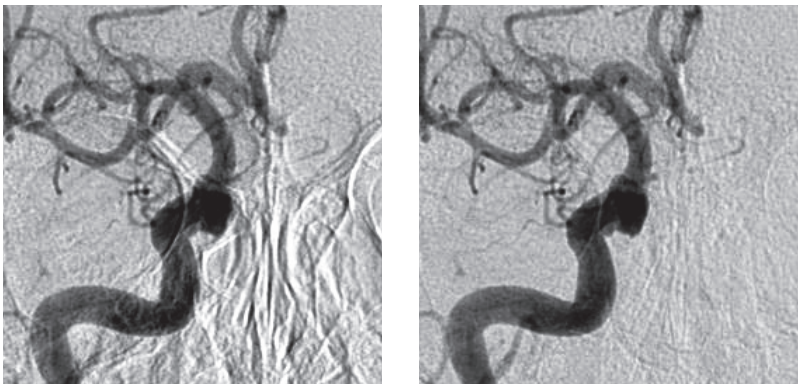

Fig. 2 Example of Microscopic Blood Vessels Visibility Improved by Flex-APS
(Left: without Flex-APS, Right: with Flex-APS) * Shows a part of a 12-inch field of view image.

3 Utilizing the Multi Data Fusion Protocol

SCORE 3D Workstation, which is the 3D workstation for Trinias series systems, has a multi data fusion protocol that enables to display and process multiple sets of data together. This function is used to merge different sets of data of a same patient in three-dimensional space and display volume-rendered (VR) images. This multi data fusion protocol can be used for up to four different sets of data.

They utilize this function to create a variety of images for different purposes. For example, in the case of intracranial aneurysm, they create a fusion image of the internal carotid artery acquired by 3D-DSA and the bone acquired by SCORE CT in order to make it easier to understand visually positional relationship of the arterial aneurysm and the skull base. Similarly, they merge the data of the internal carotid artery and that of the bone to create an image which can be used to simulate the situation of a craniotomy surgery by making a virtual hole on the skull in the case of arteriovenous malformation (AVM), which is shown in **Fig. 4**. **Fig. 5** shows an image of d-AVF case. It enables to display feeder vessels extended to a shunt on the top of head from left and right in one image by merging contrast images of left-CCA and right-CCA. This feature has been appraised as follows, “It has a wide range of uses, including the production of images to assist complicated surgical procedures. If there are opportunities, we are looking forward to using the multi data fusion protocol in other cases of complicated treatment procedures that has not been used before in the clinical area.”

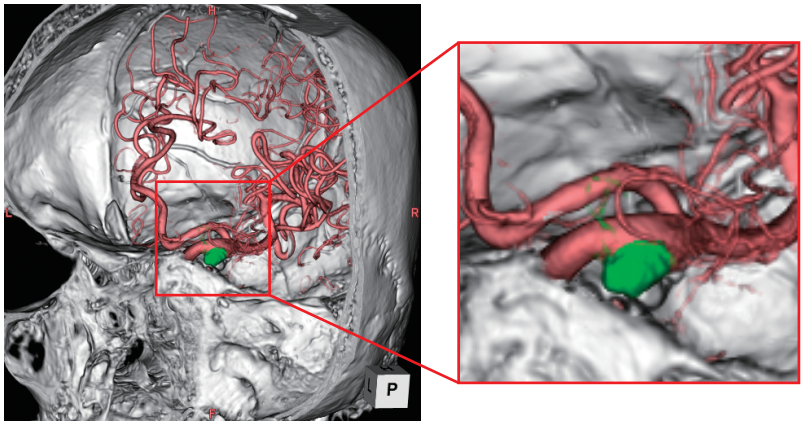

Fig. 3 Fusion Image Showing the Right Internal Carotid Artery (3D-DSA) and the Skull (SCORE CT) of a Patient with a Brain Aneurysm

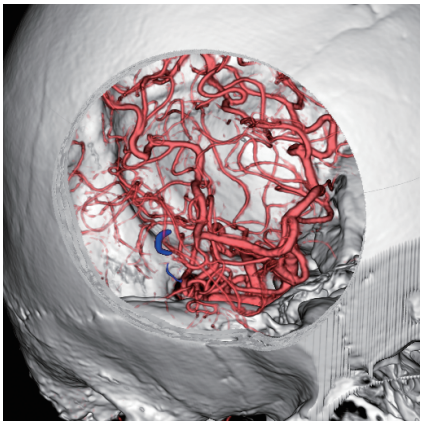

Fig. 4 Fusion Image Showing the Right Internal Carotid Artery (3D-DSA) and the Skull (SCORE CT) after the AVM Embolization procedure

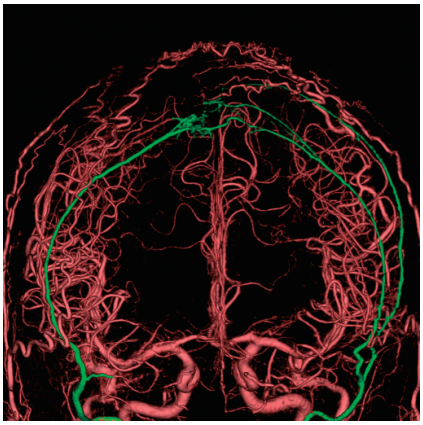

Fig. 5 Fusion Image Showing Left and Right Common Carotid Arteries (3D-DSA) of a Patient with d-AVF

Reference

1) Masayuki Yasumi, Trinias Family of Angiography Systems—Latest Technological Development in SCORE Imaging, MEDICAL NOW, No. 82, 11-13, 2017

Stories of Kyoto-born Masterpieces — 22

Numerous outstanding products have helped shape the history of Kyoto — here we outline the stories hidden behind them.

Warosoku are sold by an old Japanese unit of weight, momme. Only fixed weights are sold: 20 momme of white *bogata* and *ikarigata*, 10 momme of white *bogata*, and 20 or 30 momme of red *ikarigata*. The candle on the right is used for evening tea ceremonies, and is known as a *sukiya* candle.

Kyoto-made Warosoku

Large, gentle, irregularly flickering orange flames—these *warosoku*, or Japanese candles, have long illuminated daily lives and been offered to Shinto and Buddhist deities.

Warosoku are made from plant-based wax. The highest quality of these Japanese candles use wax made from the fruit of the Japanese wax tree (*mokuro*), while others use wax from honey bee nests or rice bran wax. Moreover, the wicks of these candles use Japanese *washi* paper and *igusa* grass, meaning the entire candle is created from natural materials. Craftsmen produce each candle by hand, and they are sold for high prices. On the other hand, Western candles are made using paraffin wax from petroleum and use string for their wicks. They can be mass-produced , and be acquired relatively cheaply. With the proliferation of electricity, traditional Japanese *andon* lamps are now obsolete, and the candles used in Buddhist and Shinto household altars and at gravesides now are predominantly Western candles.

Differing production methods depending on the shape

The reason that *warosoku* have survived even as times have changed is the high demand from temples. *Warosoku* generate little smoke and soot and thereby minimize stains on objects of worship, while the minimal flickering of their flames allows undisturbed chanting of sutras. As such, candles of differing sizes and weights are produced to match temples' various candle holders.

Warosoku come in two shapes: *bogata*, which narrow in shape from top to bottom, and *ikarigata*, which somewhat resemble a shamisen pick, and widen both at the top and the bottom. The methods to create the core of each are different. *Bogata* candles are made through a process known as *kigake*, in which the wicks are attached to bamboo spits. Craftsmen turn a number of these spits in their right hand while layering melted wax onto them with their left hand. This ensures that each candle consists of multiple layers for a stunning finish. *Ikarigata*, meanwhile, are created through a process known as *ikomi*, in which melted wax is poured into a wooden mold to create each candle. *Ikarigata* candles are predominantly used in the Jodo Shinshu school of Buddhism.

The wicks of both types of *warosoku* candles are created from a cylindrical piece of *washi* paper upon which *igusa* grass is closely wrapped. To ensure the *igusa* grass doesn't break, the craftsmen spray mist onto the cylinder as it is wrapped, before fastening it with silk floss. The wrapping of the wick is adapted to the condition of the season's *mokuro* wax—if the wax is soft, for example, the grass is tightly wrapped to ensure the wax stays

The workshop is home to various *ikomi* molds—some are over 400 years old, while others are only used for special anniversaries once every 50 years.

Air is kneaded into the melted wax with a thick bamboo pole to generate the perfect consistency.

The final *uwaro* layer is applied using the *kigake* method. Applying too much wax will mean the candle won't have a clean white finish. After, the top and bottom are cut to shape.

The wax is ignited, and the flame gets bigger as the wick begins to absorb air and wax.

Spits are wrapped in *washi* paper and *igusa* grass to create the wick. Prior to the peak season, the fourth-generation Tanji craftsman is in charge of wick-making.

A vermilion-colored *ikarigata* candle is painted onto a store sign.

attached to the cylindrical core. The end is fixed with wax, and after final adjustments to ensure the shape is maintained, the wick is complete.

Third-generation head of Tanji Renshodo, Kiyoshi Tanji, says this: "To create the core, the *ikomi* method might seem easier than the *kigake* method, but actually this isn't the case." The melting point of haze wax—that from the Japanese wax tree—is 52°C, and so after melting the wax at low heat, it is slowly cooled until it is of a syrup-like texture, before being poured into the mold. Judging the hardness of the wax, therefore, is no easy task. Further, each of the wooden molds is slightly different in shape, and so once the wax is removed, the curves of each are modified with a small knife to ensure consistency. This process is known as *aburanuki*, and enables the final layer of wax (*uwaro*) to be applied beautifully. In some cases, *ikarigata* candles are finished at a later date with another layer of vermillion wax, with each layer just 1 mm thick. This stunning, uniform layering can only be achieved by hand. Moreover, only one process can be carried out each day, meaning that a single candle is complete in around 7 to 10 days.

Continued production for use at temples

Tanji Renshodo was established more than 80 years ago, and its store is located nearby Higashi Hongan-ji Temple, the head temple of the Otani sect of Jodo Shinshu Buddhism. When a former candle shop failed (it had been running for three generations prior), the first-generation head, who was working as a head merchant, took on the candle production work for Higashi Hongan-ji Temple. As a store that produces *warosoku* candles, essential for use in temples, Tanji Renshodo has earned strong trust, and receives a fixed number of orders from temples nationwide each year. Third-generation head Kiyoshi Tanji says, "Although other stores making *warosoku* for *andon* lamps have gradually closed, we've managed to continue through our supply to temples."

The fourth-generation Tanji craftsman now works with him in the workshop, but still isn't allowed to apply the final *uwaro* layer. Even with 15 years of training, applying the finishing layer just by feel is too much of a challenge.

The 470-year-old store sign hanging on the wall reads *seijo kigake*. This refers to a store that uses pure haze wax, *igusa* grass, *washi* paper, and silk floss as materials to create candles using the *kigake* technique. So as to do the signboard proud, the store continues to wholeheartedly create the highest quality *warosoku* for temples around Japan, with only the finest *mokuro* wax.

Special thanks to: Tanji Renshodo; +81-75-361-0937

R/F

Benefits of Tomosynthesis for Diagnostic Imaging of Fresh Vertebral Fractures

Eiichiro Iwata,
M.D., Ph.D.

Department of Orthopaedic Surgery, Nara City Hospital[1],
Department of Radiology, Division of Medical Technology, Nara City Hospital[2],
Department of Orthopaedic Surgery, Nara Medical University[3]

Eiichiro Iwata[1], Takeshi Kuzuwa[2], Takuya Jo[1], Yoshiyuki Konishi[2], Hiroshi Yajima[1], and Yasuhito Tanaka[3]

1. Introduction

Fresh vertebral fractures often only exhibit mild vertebral collapse at initial examination and are often difficult to discern with radiography. Tomosynthesis (TOMOS) is a tomographic imaging method that uses X-rays and, like CT, allows the evaluation of coronal-sectional slices of the vertebra and can even potentially diagnose vertebral fractures with mild collapse.

2. Objective

The objective of this study was to compare the benefits of radiography and TOMOS in the diagnosis of fresh vertebral fractures.

3. Subjects and Methods

This study included consecutive patients aged 70 years and older who visited our hospital complaining of low back pain between February and September in 2018. At initial examination, we performed frontal view and lateral view radiography and frontal view and lateral view TOMOS in the supine position and the decubitus position. Plain MRI was also performed in all patients within 2 weeks of initial examination for a definite diagnosis of fresh vertebral fractures. Fresh vertebral fractures were diagnosed by TOMOS based on the report by Otake et al[1] **(Fig. 1)**. The sensitivity and specificity of fresh vertebral fracture diagnosis were calculated for radiography and TOMOS. The positive diagnosis rate for fresh vertebral fracture was also calculated for both radiography and TOMOS. For the statistical analysis, the chi-squared test was used and a significant difference was determined based on $P < 0.05$.

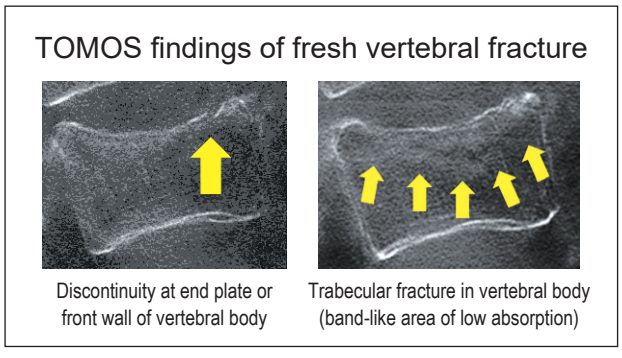

Fig.1 TOMOS Findings of Fresh Vertebral Fracture
(Quoted from Otake et al, MEDICAL NOW, No. 82, 2017.)

4. Results

Eighteen cases were included in this study. Of these cases, 10 (56%) were given a definite diagnosis of fresh vertebral fracture based on plain MRI. The [sensitivity, specificity, and P-value] results for radiography and TOMOS revealing fresh vertebral fractures in these 10 cases were [30%, 100%, and P = 0.09] and [80%, 75%, and P = 0.02], respectively **(Table 1)**. Also, among the 10 cases with a fresh vertebral fracture, the positive diagnosis rate for radiography was 30% (3 cases) and for TOMOS was 80% (8 cases) **(Table 2)**.

Table 1 Sensitivity and Specificity of Radiography and TOMOS for Fresh Vertebral Fracture

	Sensitivity	Specificity	*P*
Radiography	30%	100%	0.09
TOMOS	80%	75%	0.02*

Statistics: Chi-square test

Table 2 Positive Diagnosis Rate of Radiography and TOMOS for Fresh Vertebral Fracture

Among 10 cases with fresh vertebral fracture	
Radiography	3 cases
TOMOS	8 cases

5. A Representative Case

An 80-year old woman had a backache while lifting a futon. She visited our hospital the following day and radiography and TOMOS were performed during the initial examination. Radiography did not identify

a fresh vertebral fracture but TOMOS lateral view images revealed a discontinuity at the upper and lower edge of the end plates of the fourth lumbar vertebra **(Fig. 2)**. A MRI was performed 1 week later and led to a definite diagnosis of fresh vertebral fracture of the fourth lumbar vertebra **(Fig. 3)**.

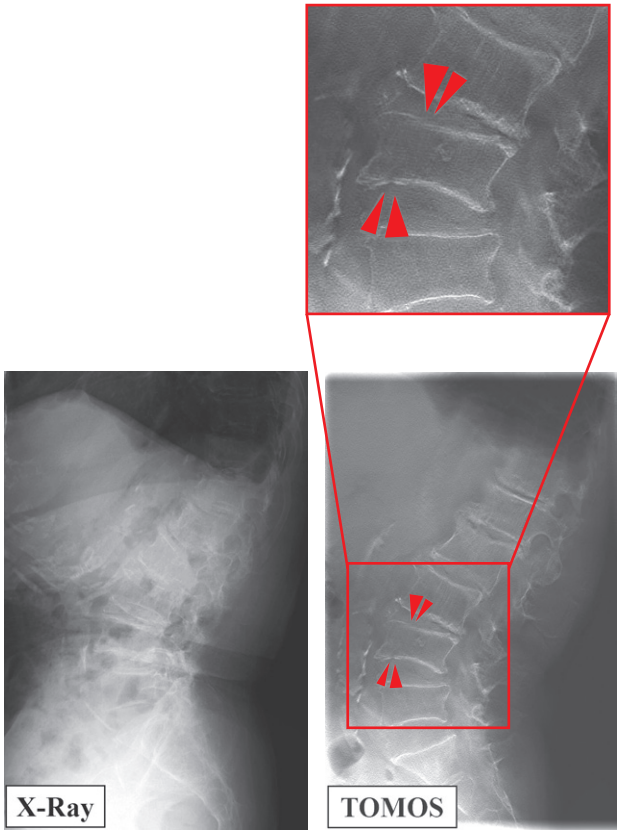

Fig.2 Radiography and TOMOS Lateral Views during Initial Examination of an 80-year-old Woman
Left: Radiographic images do not show clear findings of a fresh vertebral fracture.
Right: TOMOS images show a discontinuity at the upper and lower edge of the end plates of the fourth lumbar vertebra (red arrows).

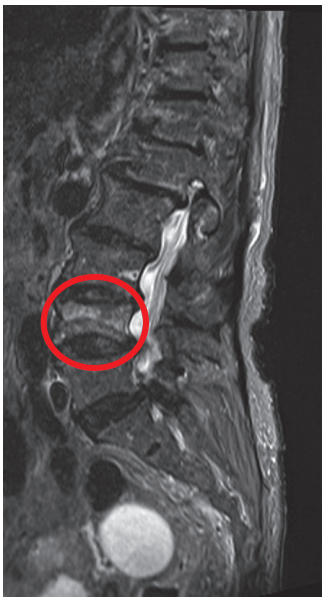

Fig.3 MRI of the 80-year-old Woman Performed 1 Week after Initial Examination
Fresh vertebral fracture shown in fourth lumbar vertebra.

6. Discussion

Fresh vertebral fractures are present in 56% of elderly patients aged 70 or older who complain of low back pain, which is considered a high rate of incidence. Consequently, fresh vertebral fractures must be considered when examining an elderly patient complaining of low back pain. Nakano et al. report that radiography performs poorly in fresh vertebral fracture diagnosis with a very low sensitivity of just 35%[2]. This study also revealed a very low sensitivity and positive diagnosis rate of 30% for radiography in identifying fresh vertebral fractures. Therefore, diagnosis by radiography alone is likely to lead to a high number of missed cases. Radiography is also reported to have difficulty distinguishing between a fresh fracture and an old fracture when a patient has both a mild fracture and a previous fracture, and MRI is the ideal choice for patients with a suspected vertebral body fracture based on their current history or physical findings[3]. However, since not all facilities are capable of performing MRI and due to limiting cost aspect, it is not practical to perform MRI in all elderly patients with low back pain. Given a definite diagnosis of fresh vertebral fracture based on MRI findings, diagnosis by CT is reported to exhibit high sensitivity (89%), high specificity (99%), and also good reproducibility[4]. CT imaging also has the advantage of being easier to perform than MRI. However, despite recent relative improvements, patient exposure is still a problem with CT. TOMOS is reported to have a lower exposure dose than CT[5] and TOMOS imaging is also simpler than CT imaging. The results of this study showed the TOMOS sensitivity and positive diagnosis rate were both high at 80%, and TOMOS missed far fewer cases than radiography. Therefore, diagnosis by TOMOS at initial examination is considered useful for patients with a suspected fresh vertebral fracture.

7. Conclusion

1. Radiography has a low positive diagnosis rate for fresh vertebral fractures and is highly likely to miss these fractures.
2. Diagnosis by TOMOS at initial examination is considered useful for patients with a suspected fresh vertebral fracture.

References

1) Yuya Otake, Mitsutoshi Moriya, Wataru Saito, et al.: Evaluation of thoracolumbar vertebral fractures using tomosynthesis, MEDICAL NOW, No. 82, 28-29, 2017
2) Tetsuo Nakano, Yasuyuki Abe, Yasuhiro Shimizu, et al.: Rate of correct diagnosis for vertebral fracture by plain roentogenograms, Journal of Japanese Society for Fracture Repair, Vol. 21, 586-588, 1999
3) Pham T, Azulay-Parrado J, Champsaur P, et al. "Occult" osteoporotic vertebral fractures: vertebral body fractures without radiologic collapse. Spine. 2005;30:2430-5.
4) Karaca L, Yuceler Z, Kantarci M, et al. The feasibility of dual-energy CT in differentiation of vertebral compression fractures. Br J Radiol. 2016;89:20150300.
5) Koyama S, Aoyama T, Oda N, et al. Radiation dose evaluation in tomosynthesis and C-arm cone-beam CT examinations with an anthropomorphic phantom. Med Phys. 2010;37:4298-306.

R/F

A Study of Pediatric Fluoroscopic Examinations
(A Method of Dose Reduction with a Removable Anti-Scatter Grid and Selectable Multi Beam Hardening Filter)

Yuki Tsuchiya, R.T.

Department of Radiological Technology, Division of Medical Technology, Fussa Hospital
Yuki Tsuchiya

1. Introduction

Fussa Hospital, located in the western part of the Tama area of Tokyo, is a core hospital with 316 beds and responsible for community medicine in two cities (Fussa City and Hamura City) and one town (Mizuho Town). 15 radiological technologists and 2 radiologists in the Department of Radiological Technology, the Division of Medical Technology work full-time. We perform various types of general radiography, fluoroscopic exam, mammography, dental radiography, lithotripsy, CT, MRI, diagnostic imaging, nuclear examination and therapy, radiotherapy, and angiography (IVR) **(Fig. 1)**.
In October 2008, the hospital reopened after renovations and the majority of its diagnostic imaging systems were converted to FPD-equipped systems. Our R/F systems is renewed in 2018, and various fluoroscopic examinations are carried out by introducing 3 of Shimadzu's SONIALVISION G4 systems. One of these systems is equipped with Tomosynthesis and SLOT radiography and works in the field of orthopedics where it performs digital tomography on various joints, SLOT radiography of full spine and full leg, and other applications **(Fig. 2)**.
At our hospital, fluoroscopic examination is utilized by a wide range of departments such as surgery, orthopedics, urology, pediatrics, gynecology, and internal medicine. In particular, pediatric urological and surgical examinations are actively performed and our R/F systems are in full use (for voiding cystourethrography, pediatric enema, GI exam, etc.).

2. Background

Fluoroscopy has been performed in all age groups, however, examinations in pediatric include examinations and radiography using other modalities and multiples examinations may be performed. Needless to say, there is a high risk of radiation injury for patient's future, and it is essential to reduce the exposure dose. In addition, there are papers and discussions that suggest the risk of inducing childhood cancer worldwide.
The SONIALVISION G4 systems which our hospital introduced this time, have a removable anti-scatter grid function and a selectable multi beam hardening (BH) filter function, and it has the possibility of drastic dose reduction.
Both physicians and nurses are involved in pediatric fluoroscopic examinations, and reduction of exposure dose for operators and medical staffs is also an issue in this field. In December 2018, our hospital

Fig.1 View of Fussa Hospital

Fig.2 SONIALVISION G4

was certified as a facility of radiation exposure reduction and is actively working to reduce exposure not just in pediatric medicine, but for all examinations and in all medical fields.
In this paper, we report the result of an investigation of an examination environment for pediatrics that minimizes dose while maintaining image quality.

3. Removable Anti-Scatter Grid and Selectable Multi Beam Hardening (BH) Filter

The SONIALVISION G4 systems introduced this time can manually detach the anti-scatter grid. BH filters can also be changed on the SONIALVISION G4 control console. The anti-scatter grid has a grid ratio of 10:1, uses an aluminum interspacer, and has 44 lines/cm at a focal distance of 120 cm. The grid can be installed and removed manually with ease from the side of the main unit of the system. The grid can be removed simply pulling it out and it can be fixed without stress even in the reinsertion **(Fig. 3)**.
Three different BH filters can be selected from the touch panel on the console: 0.1 mm, 0.2 mm, and 0.3 mm Cu. There is also an option to use no BH filter. These options can be selected during an examination with a single tap on the touch panel **(Fig. 3)**.

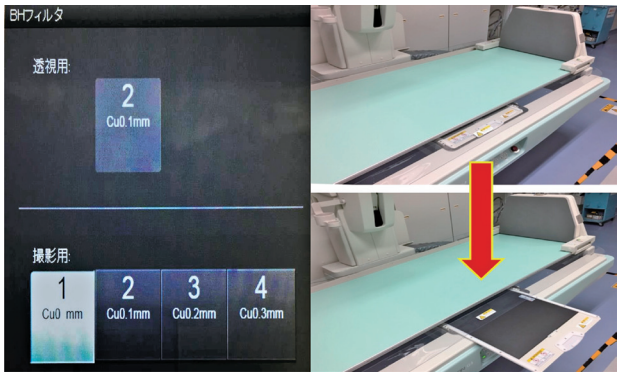

Fig.3 Console View of Selectable multi BH Filter Options (Left) and Anti-Scatter Grid Installation Method (Right)

The source-image distance (SID) of the system can also be set to 110 cm, 120 cm, and 150 cm and exposure dose of patient can be reduced by using a longer SID. And this function is also one of the feature of SONIALVISION G4 that the examinations can be performed so that the X-ray tube may not interfere the operator in the special examination environment of pediatrics.

4. Investigation Methods

In order to search for the optimal examination environment for pediatrics, the measurement experiment of the following items was carried out in total 8 kinds of combination of the anti-scatter grid with or without and with four different BH filter configurations (none, 0.1 mm, 0.2 mm, and 0.3 mm) including the usual examination settings. The usual examination setup is with an anti-scatter grid and no BH filter.

1. (1) Entrance surface dose, (2) Dose-area product, (3) Fluoroscopy tube voltage, (4) Fluoroscopy tube current, and (5) Fluoroscopy dose rate.
2. (1) Contrast-to-noise ratio (CNR) and (2) Figure of Merit (FOM)
3. Visual evaluation of Burger phantom **(Fig. 4)**
4. Visual evaluation of human phantom **(Fig. 4)**

Visual evaluation of a Burger phantom was performed on 8 images taken under each condition by 15 radiological technologists at our hospital **(Fig. 4)**.

Fig.4 **a)** Burger Phantom Measurement Method
b) Human Phantom Measurement Method
c) Visual Evaluation of Burger Phantom
d) Visual Evaluation of Human Phantom

For visual evaluation of the human phantom, wrist joint human phantom was used in place of an infant's body. In the usual examination setting (With grid and no BH filter), our hospital's 15 radiological technologists performed a 5-point evaluation on 7 images taken under each conditions.

The evaluation items are following 1 ~ 5 items and overall balance, 6 items in total.

In this evaluation, since the wrist joint human body phantom was assumed to be the infant's body, each position of the wrist joint was assumed to be each position of the infant.

(1) Able to verify overlapping of the radius and navicular bone (a line at the end of the radius): trachea
(2) Able to trace the outline of the trapezium bone: gastric gas
(3) Able to trace the outline of the capitate bone: kidneys
(4) Able to verify a gap between the lunar bone and triquetral bone: ureter
(5) Able to discern a gap between the second and third metacarpal bones: intestinal tract

• Overall balance

Each of these items was evaluated on a 5-point as "inferior", "slightly inferior", "unchanged", "little better", or "better".

5. Results

1-(1) Entrance surface dose (Fig. 5 left)

The result of entrance surface dose was lower without the grid (Grid(-)) than with the grid (Grid(+)). Also, the difference by the type of the BH filter showed the greater the filter thickness the lower the entrance surface dose.

1-(2) Dose-area product (Fig. 5 right)

Similar to the results for entrance surface dose, the dose-area product was lower without the grid (Grid(-)) and the greater the thickness of the BH filter the lower the dose-area product.

1-(3)(4)(5) (3) Fluoroscopy tube voltage, (4) Fluoroscopy tube current, and (5) Fluoroscopy dose rate (Fig. 6)

As for a result of fluoroscopic parameters, because BH filter for fluoroscopy is fixed at 0.1 mm Cu due to the specification of the system, we report only the results of the difference between with / without the Grid. Fluoroscopy tube voltage, tube current, and dose rate were all lower without the grid (Grid(-)) than with the grid (Grid(+)).

2-(1) Contrast noise ratio (Fig. 7 left)

The CNR was higher with the grid (Grid(+)) than without the grid (Grid(-)) and the greater the thickness of the BH filter the higher the CNR.

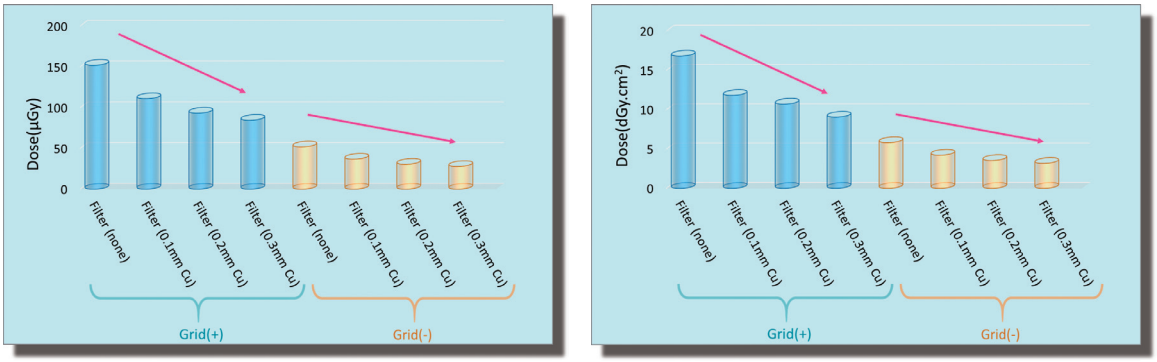

Fig.5 Entrance Surface Dose Results (Left) and Dose Area Product Results (Right)

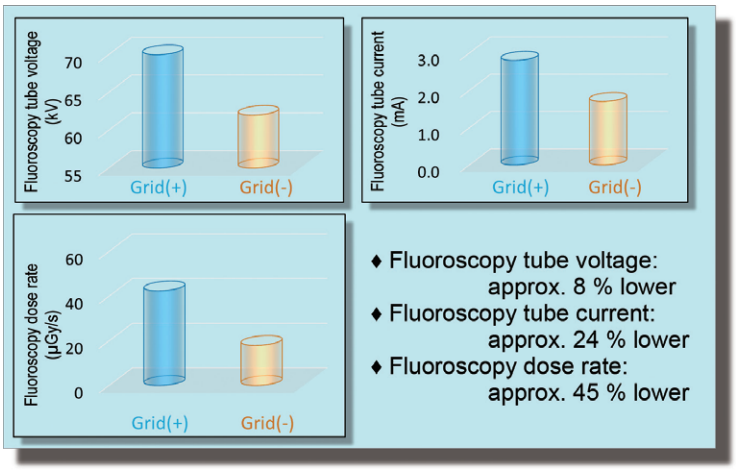

Fig.6 Fluoroscopy Tube Voltage, Fluoroscopy Tube Current, and Fluoroscopy Dose Rate Results

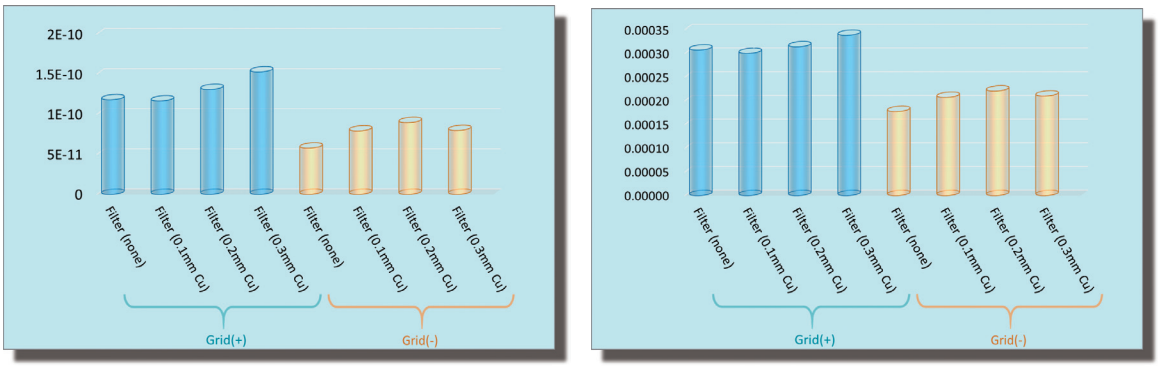

Fig.7 Contrast Noise Ratio (Left) and Figure of Merit (Right)

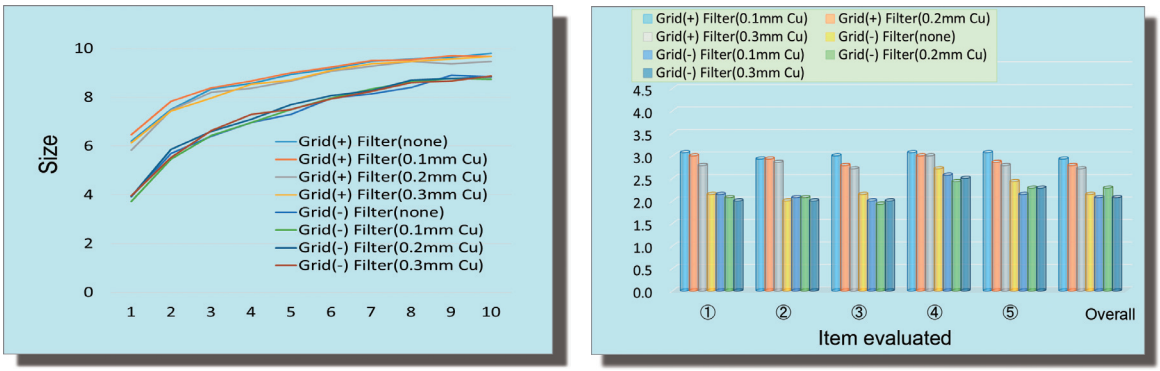

Fig.8 Visual Evaluation of Burger Phantom (Left) and Visual Evaluation of Human Phantom (Right)

2-(2) Figure of Merit (FOM) (Fig. 7 right)

Similar to the CNR, the FOM was higher with the grid (Grid(+)) and the greater the thickness of the BH filter the higher the FOM.

3 Visual evaluation of Burger phantom (Fig. 8 left)

The result of visual evaluation of the Burger phantom is with the grid (Grid(+)) resulted in a slightly better than without the grid (Grid(-)).

The difference of thickness of BH filter had no substantial effect on the visual evaluation results.

4 Visual evaluation of human phantom (Fig. 8 right)

Similar to the Burger phantom, with the grid (Grid(+)) resulted in a slightly better visual evaluation of the human phantom than without the grid (Grid(-)).

6. Discussion

- In the entrance surface dose and the fluoroscopic parameters, the effect of reduction in dose was recognized using the grid and changing the BH filter. It is considered that it is caused by lowering of X-ray condition and removal of soft X-rays by the filter.
- As for CNR, the thicker the BH filter, the slightly better the result was.

  Though CNR seemed to decrease in general, this result is probably the characteristic of this system, when it is estimated from exposure time and digital value etc.. And, it is considered that the difference of the Grid (with / without) is caused by the difference of contrast caused by scattered X-ray.
- For FOM, regardless of the Grid (with / without), the use of the BH filter gave good result.

  This result is probably due to the effect of a reduced dose and the CNR.
- As for results for visual evaluation of a Burger phantom and human phantom, the difference between the existence of the Grid was recognized. The BH filter did not affect the results from visual evaluation.

Based on the above findings, physical evaluation showed that using the BH filter was beneficial for reducing exposure dose, while visual evaluation with phantoms showed that using the BH filter had no major effect. This is considered to be an effect of limiting phantom thickness to 10 cm, because this investigation is an examination of the pediatrics. Also, though without the Grid (Grid(-)) reduced the exposure dose, it also resulted in slightly poorer results from visual evaluation. Nevertheless, since our hospital mainly uses pediatric fluoroscopic examinations to observe larger structures such as the colon and ureter rather than fine structures,

the slight reduction in image quality seen in this investigation is not enough to draw concern **(Fig. 9)**.

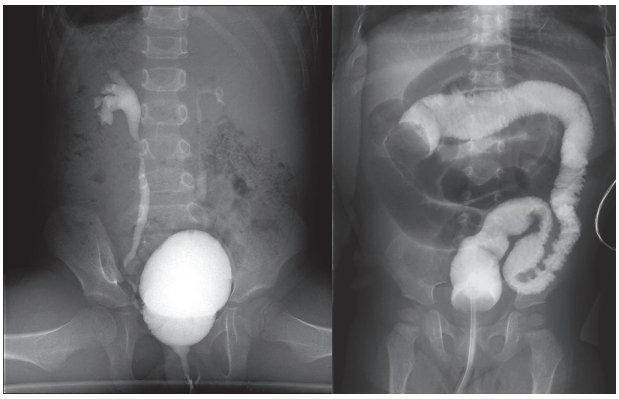

Fig.9 Clinical Images
Pediatric Voiding Cystourethrography (Left)
Pediatric Enema (Right)

7. Conclusion

Because our hospital runs rotations using different imaging modalities from one day to the next, our staff are not permanently responsible for particular modalities. For this reason, it is particularly important our medical staffs understand the details of each fluoroscopic examination before the examination. Understanding the details of an examination may avoid unnecessary fluoroscopy or radiography for an examination. In addition, using procedural functions and setting protocols for pediatric allows all the radiological technologist to carry out fluoroscopic examination in fluoroscopic condition that take advantages of the removable anti-scatter grid function and the selectable multi BH filter function. In this way, we believe we have established an examination environment that reduces the exposure dose.

In some cases in our hospital, the conditions are set for without Grid, and the thickness of BH filter is changed for each purpose of the pediatric fluoroscopic examination **(Table 1)**.

We would like to continue our efforts to further reduce the exposure dose of patients and operators, not only in pediatric examinations but for all fluoroscopic examinations.

Table 1 Examination conditions at our hospital

	Grid	Filter
Intussusception	—	0.3mm
Urinary system examinations	—	0.1mm
Reductions	—	0.3mm
Others	—	0.2mm

References

1) Yoshitaka Nakai, Cutting Edge of ERCP—Experience Using the SONIALVISION G4 and Reducing Scattered Radiation Dose Levels, MEDICAL NOW, No. 85, 18-22, 2019
2) Yoshinao Mori et al.: Low Dose Mode of SUREngine FAST Highly Rated for Use in Biliopancreatic Endoscopy, MEDICAL NOW, No. 85, 23-25, 2019
3) Junichi Hachiya et al.: Radiology Subnote, Nankodo
4) Hirotsugu Munechika (Chief Editor) and Yasuo Nakazawa (Editor), Full Course of Diagnostic Imaging for Radiological Technologists, MEDICAL VIEW, 2010
5) Keigo Endo (Chief Editor), Zukai shinryo hoshasen gijutsu jissen gaido, Bunkodo, 2014
6) Hiromu Nishitani et al.: Hyojun hoshasen igaku, Igaku-Shoin, 2011

RAD

Our Experience Using MobileDaRt Evolution MX8 k type

Hisahiro Kitai, R.T.

Department of Radiology, Shiroyama Hospital
Hisahiro Kitai

1. Hospital Overview

Shiroyama Hospital **(Fig. 1)** is located in Habikino City in southern Osaka, in an area well-loved by history mania . The hospital stands in the Habikino Hills overlooking the Furuichi Kofungun (a cluster of tumuli), now a World Cultural Heritage Site, and the nearest train station is Furuichi Station on the Kintetsu Minami Osaka Line, an area that played host to the clash between Date Masamune and Sanada Yukimura in the famous Battle of Domyoji/ Konda during the Summer Campaign of the Siege of Osaka.

Shiroyama Hospital was first established in 1978 with 156 beds on a site adjacent to Furuichi Station. In 1989 it was expanded to 299 beds, and in 2006 the hospital moved to new facilities at its current site.

Operating on the hospital motto of “Shiroyama Hospital Exists for the Patients,” we are a community-based, acute care-oriented core hospital that provides 24-hour medical care with 23 outpatient departments plus a critical care department that see 12,000 emergency patients and 140,000 outpatients each year.

In 2018, Shiroyama Hospital also accepted the request to become a Disaster Medical Center for Habikino City.

Fig.1 View of Shiroyama Hospital

2. Equipment Introduction story and Selection

Although computed radiography (CR) was used in our previous mobile X-ray system, an increasing number of technical problems stemming from aging equipment and the departments of radiology and medical examination wanting to improve imaging work efficiency led to the acquisition of a new mobile X-ray system with a flat panel detector (FPD), rather than the previous CR system.

The previous mobile X-ray CR system required the system to carry the same number of CR cassettes as the number of images taken and the aging equipment had become less maneuverable, making work difficult for radiology technologists.

Our department of radiology has 24 clinical radiology technologists of whom 9 are women. Our primary requirement for selecting a mobile X-ray system was that the equipment can be used safely and comfortably by all our staff, including female and male technologists under 150 cm and over 180 cm in height.

(1) The FPD is wireless and lightweight.
(2) The system itself comes with a built-in viewing monitor that is as large as possible.
(3) The system can access the hospital’s radiology information system (RIS) via remote desktop on site.
(4) The system allows patient authentication with a wireless bar code reader.
(5) Images can be viewed and sent to the image server immediately after acquisition.
(6) There is a wireless hand switch for exposures.
(7) As much storage space as possible for FPD device.
(8) The system is quiet during both transport and operation.
(9) The external design of the equipment does not cause concern to patients.

Fig.2 MobileDaRt Evolution MX8 k type (a) side view and (b) 19-inch touch panel viewing monitor.

We found MobileDaRt Evolution MX8 k type (hereinafter referred to as MobileDaRt Evolution MX8) met all our desired specifications noted above and chose it as our new mobile X-ray system **(Fig. 2)**.

3. Hospital Environment

The electronic medical records system (hereinafter referred to as hospital information system [HIS]) at Shiroyama Hospital is made by Software Service, Inc., our image server, in-hospital distributed image viewers, and image reading and reporting system is made by PSP Corporation, and our Radiology Information System [RIS] is made by Infocom Corporation. The hospital operates a wireless local area network (LAN) that allows order information on the RIS to be downloaded wirelessly by remote control and viewed on mobile systems, and after imaging allows the resulting images to be immediately transferred to the image server from anywhere in the hospital.

4. Workflow

We mainly use MobileDaRt Evolution MX8 in hospital wards but also sometimes use it in operating rooms and emergency rooms.
The imaging workflow is shown below.

(1) A doctor orders a radiography at the ward via HIS.
(2) Order information and patient information are verified in the RIS terminal screen shown on the MobileDaRt Evolution MX8 built-in monitor and the system is transported to the radiography site.
(3) At the bedside of the radiography subject, the bar code on the patient's wristband is read using the wireless bar code reader that comes with the system. Upon reading the bar code, patient information is identified in the RIS terminal screen from the radiography schedule patient list, and after checking patient information and order details, radiography request procedures are followed on the RIS terminal screen.
(4) The radiography screen is then activated and radiography is performed.
(5) After performing radiography, an image inspection is performed immediately using the built-in monitor, and after image processing and annotation are complete, the radiography images are transmitted to the image server over the wireless LAN.
(6) After using the RIS terminal screen shown on the built-in monitor to confirm that images successfully reached the image server, an imaging termination process (post-imaging processing) is implemented.

5. Our Experience Using MobileDaRt Evolution MX8

● Telescopic column and motor-assisted transport

Our previous mobile X-ray system included a long, wide column that stood directly in front of the operator and obstructed their view during transport. The column forced even tall technologists to lean around the column and adopt an unnatural body position to see in front of the system when holding the transport handle, and to be very cautious when transporting the system.
A distinguishing feature of MobileDaRt Evolution MX8 is its telescopic column that does not obstruct the technologist's field of view during transport so even smaller technologists under 150 cm in height can transport the system safely through the hospital with a natural body posture **(Fig.3, 4)**.
The low center of gravity of the system combined with the smoothness of its motor-assisted drive mechanism allows all technologists, both men and women, to perform radiology rounds easily, safely, and without stress.

Fig.3 Forward View during Transport

Fig.4 The telescopic column lets smaller radiology technologists transport the system safely and with a relaxed posture.

● X-ray tube support arm operations

Many mobile X-ray systems require adjustment of several screws to adjust or lock the X-ray arm, but all arm articulations in this system can be released (“all free”) or locked (“all locked”) with the press of a single button, which allows for smooth arm position adjustments **(Fig. 5)**.

It is incredible how easy the arm can be manipulated by all technologists in our department.

Fig.5 “All free” switch

● Transporting noise and operating noise

The new system is incomparable to the old system in how quiet it remains during transport.

The system is so quiet we now face the danger of people being unaware of an approaching system during daytime ward rounds when human traffic is high. To be safe, we sometimes need to alert people to the presence of the system when transporting it through ward corridors in the daytime. For this reason, our system can be configured to play a warning sound that is also adjustable for volume.

System settings also allow us to mute the warning sound and other operating and control sounds depending on the time of day, so at night the system can be muted completely other than the warning sound used to indicate X-ray exposure.

This feature is useful when transporting the system through wards at night or performing radiography in shared rooms, and is used all the time at our hospital.

● Instantaneous image verification and ease of repeat radiography

While not a frequent occurrence, repeat radiography is sometimes inevitable in the course of radiography work.

The built-in monitor on MobileDaRt Evolution MX8 can be used to verify images immediately after acquisition so examinations can be completed without repeated ward visits, thereby reducing the workload for technologists, for nurses assisting with radiography, and for patients undergoing repeat radiography.

Recently, mobile X-ray systems are often used as a safety measure to verify the position of intubation tubes and other devices inserted in the body. At our hospital, doctors will immediately check images on the built-in monitor, and if tube positioning is not satisfactory will adjust it there and then without removing the FPD from the patient and immediately perform another exposure to check the results.

This feature is highly rated by both the clinical department (doctors) and the nursing department (nurses).

● Work efficiency

With a wireless LAN, the system can be used to obtain order information, transfer images to the image server, and even let the person performing radiography see additional radiography orders during daytime rounds. This has removed the need for doctors, nurses, and our department reception to personally contact the person performing radiography about additional radiography orders.

The person performing radiography also no longer needs to return to our department to pick up additional cassettes. There are no longer situations that the technologist has to run back to the CR reading room holding the CR cassette to get printed images in a hurry, leaving the mobile X-ray system behind.

● Wireless hand switch (optional) (Fig. 6)

The wireless hand switch can be used to increase the distance between the technologist and the patient when performing exposures and reduce exposure for the technologist.
Previously, the hand switch cable sometimes required extra attention during radiography that involved patient assistance, but the wireless hand switch solves this problem and has proven to be extremely convenient.

Fig.6 Wireless hand switch

● Wireless bar code reader (optional) (Fig. 7)

Patients can be matched to a radiography order by reading the bar code on the wrist strap worn permanently by the patient. This helps not only to reduce work in preparation for imaging but also to prevent patient misidentification.

Fig.7 Wireless bar code reader

● Storage bin (Fig. 8)

The system comes with a large amount of storage bin that is extremely useful not only for carrying grids, but also for wet wipes, plastic bags to protect FPDs, and other materials used during radiography.

Fig.8 Storage space

● Decorated version (Fig. 9)

Patients have told us that seeing the machine entering their room makes them nervous and afraid, as does seeing the large, mechanized device approaching them anywhere in the hospital.
To alleviate this nervousness even just a little, the exterior of the system has been decorated with stickers of animals and dessert foods.
Extending the system arm now reveals cute monkeys and also extends the giraffe's neck.
Matching this theme, the protective clothing worn by technologists operating the mobile X-ray system also has a giraffe pattern.
Somewhat unexpectedly, the decorated system has been universally well-received by inpatients (including patients not being examined), patient

Fig.9 Decorated version

Fig.10 Driving handle height adjustment

attendants, visitors, and also other hospital staff who frequently smile when they see the decorated system.
The decoration also attracts peoples' attention during radiology rounds, though this is an acceptable side effect.
It is perhaps worth noting that our hospital has no pediatric outpatient department or pediatric wards.

● Height-adjustable steering handle (optional) (Fig. 10)

Technologists of many different statures (male and female) perform mobile radiography work, so the ability to adjust the height of the steering handle (two levels) helps technologists who were otherwise forced to adopt an unnatural body position while moving the system, and therefore reduces the physical burden on technologists.

6. Summary

At Shiroyama Hospital, we have acquired the MobileDaRt Evolution MX8 k type (combined with a Konika Minolta CS-7) system made by Shimadzu Corporation. Changing from a CR system to an FPD system has allowed us not only to carry out radiology rounds with a single FPD but also to verify images immediately after radiography and send images to the image server from the bedside. These improvements make radiography work easier for our radiology technologists and bring substantial time savings to mobile radiography tasks.
Technologists can now complete their scheduled mobile radiography work and return to the radiology department earlier, leaving more time to deal with other tasks and thereby increasing the overall work efficiency of the radiology department.
Before acquiring this system, our workflow after imaging involved scanning the imaging plate (IP) and sending the scanned image to the image server, which took around 10–15 minutes between imaging and being able to view the image on the HIS. With MobileDaRt Evolution MX8, images can now be viewed on the HIS within 1 minute of imaging, reducing significantly the time between imaging and image viewing and even improving the work efficiency of our doctors.
On a full charge and assuming motor assistance is not used, in 2.5 hours of digital radiography (DR) we can acquire around 150 images at 100 kV and 4 mAs, which makes MobileDaRt Evolution MX8 extremely well-suited to a Disaster Medical Center like ours.

The irradiation field adjustment knob, irradiation field lamp switch, quick switches, and inclusion of multiple arm lock release buttons in different locations on the system also constantly remind us of the clever design details that have gone into this excellent mobile X-ray system.
When it comes to Shimadzu, we would expect nothing less.

Universal Tomosynthesis Imaging with UT-Station

Medical Systems Division, Shimadzu Corporation
Junya Yamamoto

1. Introduction

Tomosynthesis is a medical term created from the words tomography and synthesis that refers to a technology for reconstructing tomographic images from multiple, consecutive radiographic images. Tomosynthesis mainly finds use in orthopedic medicine for detailed observation of fracture lines and follow-up after joint replacement surgery. Current products from Shimadzu that can perform tomosynthesis are the SONIALVISION G4 (R/F system) and the RADspeed Pro EDGE package (general radiography system). Aiming to expand the usefulness of tomosynthesis and make the technology easier to use, we have developed UT-Station, a program that realizes “universal tomosynthesis imaging” and enables tomographic images to be acquired on various radiographic imaging systems by imaging a patient together with a specially designed phantom then processing the images on a dedicated workstation. This article briefly describes universal tomosynthesis imaging with UT-Station.

2. Background

With tomosynthesis, images can be acquired without overlapping bones and tissue and allowing good confirmation of fracture lines difficult to visualize by radiography alone. Conventional tomosynthesis image reconstruction requires a flat panel detector (FPD) that can accommodate consecutive imaging and a precision mechanical control mechanism to move the imaging system in precise accordance with positional information calculated in advance based on the operational settings of the radiography system. These requirements limit which systems are capable of performing conventional tomosynthesis imaging. In universal tomosynthesis imaging, geometric positional information about the imaging system is detected from the images to be used in tomographic image reconstruction, making it possible to perform tomosynthesis imaging even on radiography systems that are not designed with a dedicated mechanical control mechanism.

3. Characteristic Features of Universal Tomosynthesis Imaging

Universal tomosynthesis imaging requires three things: (1) the UT-Station program designed for radiographic diagnostic system workstations, (2) a computer installed with UT-Station to be used as a workstation to view images and reconstruct tomographic images, and (3) a UT-phantom to

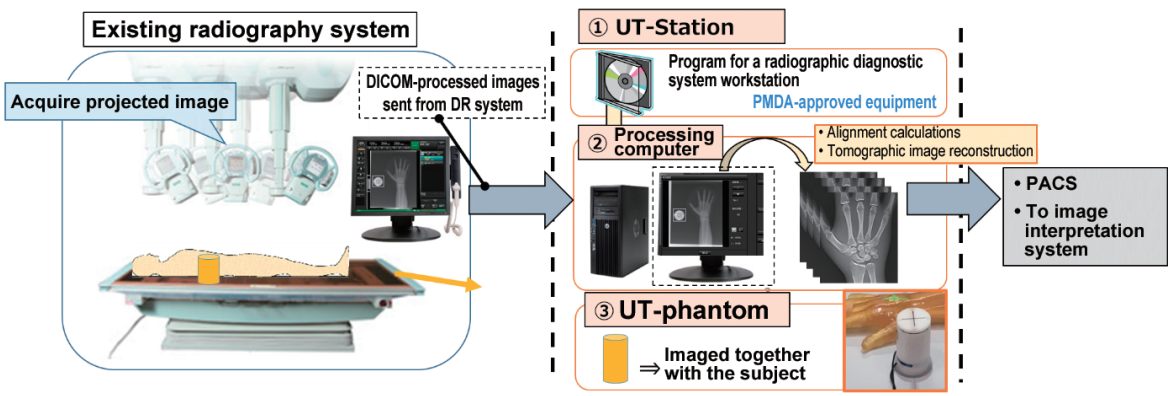

Fig.1 Overview of universal tomosynthesis imaging

obtain geometric positional information about the imaging system from acquired images. Each of these things works independently of the radiography system, so each is easily combined with an existing radiography system. An overview of universal tomosynthesis imaging is shown in **Fig. 1**. First, the UT-phantom is placed next to the subject and 5–7 radiographic images are acquired at different irradiation angles. These radiographic images are sent to the computer installed with UT-Station, and using a tomographic reconstruction function for universal tomosynthesis imaging, UT-Station performs automatic alignment calculations and tomographic image reconstruction processing. The main target of this study is the evaluation of fractures in the extremities and hip joints. The characteristic features of universal tomosynthesis and conventional tomosynthesis are shown in **Table 1**

3.1 Imaging the Subject and the UT-Phantom

For universal tomosynthesis, the FPD is mounted on the table or in the bucky and remains immobile while imaging is performed by moving the X-ray tube. The UT-phantom must be within the projected image for the entire series of acquired images, so the lines printed on the top surface of the UT-phantom are used as a guide and placed within the irradiation field as shown in **Fig. 2(a)**. As also shown in **Fig. 2(b)** and **(c)**, the base of the UT-phantom has a suction cup design and stays firmly in place on the table surface or FPD surface even during imaging in an upright position. After setting the UT-phantom in place, about 5–7 projected images are acquired with the X-ray tube system in different positions. About 1–2 minutes of imaging time is normally needed to acquire these images with a general radiography system, so immobilizing the subject with sandbags or support apparatus is more important during universal tomosynthesis imaging than during conventional tomosynthesis. Furthermore, the irradiation dose per image acquisition is smaller than normal radiography, and the total dose for an examination is as small as around 1.5–2 times a general radiography examination. Positional information about the imaging system is calculated automatically from the projected image, which means the X-ray tube does not need to be positioned precisely between each image acquisition. The RADspeed Pro (general radiography system) also has an auto-positioning function (optional) that can position the X-ray tube by remote control.

Table 1 Comparison of universal tomosynthesis and conventional tomosynthesis

	Universal tomosynthesis	Conventional tomosynthesis
FPD	Continuous imaging function not needed	FPD capable of continuous imaging
Mechanical control	Unnecessary	High-precision automatic control mechanism
Number of projected images	5–7 images (20 degrees)	20–74 images (20–40 degrees)
Imaging flow	Auto-positioning function/Manual operation	1 switch (setup → exposure)
Imaging time	Around 1–2 minutes	Around several seconds to several tens of seconds
Imaging sites	Sites with little body movement (extremities or hip joints)	No restriction
Cost	Cheaper than standard	Standard

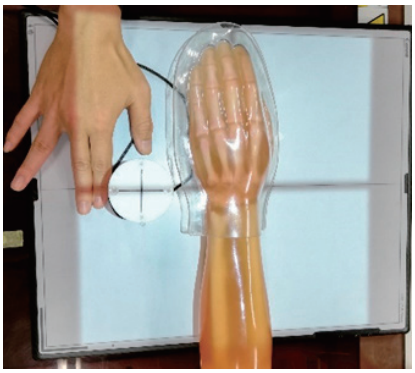

(a) Preparing irradiation field

(b) Ready for decubitus imaging

(c) Ready for upright imaging

Fig.2 Preparing the UT-phantom

3.2 Position Detection by UT-Station

Projected images sent to UT-Station from the radiography system are selected for reconstruction processing. The UT-phantom contains multiple metal markers in a prescribed positional relationship. Before reconstruction processing can commence, preprocessing automatically analyzes the position of the UT-phantom in each image and the arrangement of each metal marker in the UT-phantom, thereby calculating the position of the X-ray focal point relative to the FPD. Evaluation of three factors: accuracy of tomographic image display height, accuracy of the calculated angle of X-ray incidence in the center of the FPD, and spatial resolution of tomographic images, has verified that the position detection performed by UT-Station is equivalent in performance to tomographic images acquired by conventional tomosynthesis. Results from UT-phantom detection in each image can also be checked in UT-Station and adjusted manually **(Fig. 3)**.

3.3 UT-Station Reconstruction Algorithm

Universal tomosynthesis is based on the assumption that projected images will be acquired using an FPD for general radiography. Therefore, UT-Station has an algorithm that can handle image reconstruction from a small number of images. When tomosynthesis reconstruction is performed from a small number of projected images, the edges of cortical bone and other structures that display a large difference in luminance (high-contrast structures) cause a ripple artifact to appear on slices outside the original tomographic imaging plane. The image reconstruction algorithm used by UT-Station applies successive approximation to reduce this ripple artifact. **Fig. 4** shows images reconstructed from seven projected images using a conventional algorithm and the algorithm used by UT-Station. These images show the ripple artifact is less apparent in images reconstructed by UT-Station compared to images reconstructed using the conventional algorithm. During reconstruction, UT-Station also checks the geometric position of the imaging system based on the positional relationship of metal markers in the UT-phantom and notifies the user of errors during position detection such as might be caused by movement of the UT-phantom during imaging.

Fig.3 UT-phantom detection

4. Clinical Images

Universal tomosynthesis images created using Shimadzu's RADspeed Pro are shown in **Fig. 5**. In both images, fracture visibility is improved over radiography and even fine fracture lines are visible.

5. Conclusion

This article briefly describes universal tomosynthesis imaging. Universal tomosynthesis imaging can produce tomographic images even from radiography systems with no tomosynthesis function by determining the position of the radiographic imaging system from radiographic images. This article also describes UT-Station; a program that performs universal tomosynthesis image reconstruction and is intended

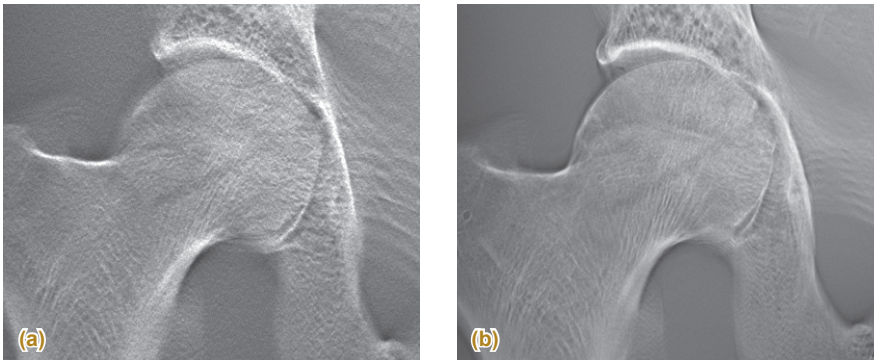

Fig.4 Ripple artifact suppression
(a) Tomographic image obtained using conventional algorithm
(b) Tomographic image obtained using UT-Station

Fig.5 Clinical case images
(a) Fracture of the right ulna
(b) Fracture of the left distal radius

for radiographic diagnostic system workstations. We look forward to being able to introduce even more new functions and applications in the future that will contribute towards more accurate diagnoses. Finally, we would like to take this opportunity to offer our sincere thanks to Yoshitami Murayama R.T., Rie Sonobe R.T., and all others involved at the Department of Radiology, Nippon Koukan Hospital for their considerable help in providing images and in clinical evaluation of universal tomosynthesis imaging, and to Takayuki Baba R.T. of the Department of Diagnostic Imaging, Imamura General Hospital for valuable advice in considering immobilization methods for imaging and in helping to create prototypes.

MEDICAL NOW Digest

www.shimadzu.com/med

6032-02902-11BTD
ISSN0916-8745